Control Scheme for Multi-Energy Microgrids with Power, Heating, Cooling, and Hydrogen Vectors

Pablo Horrillo-Quintero, Pablo García-Triviño, Ehsan Hosseini, Carlos Andrés García-Vázquez, Higinio Sánchez-Sainz and Luis M. Fernández-Ramírez

Published in:
2024 IEEE 22nd Mediterranean Electrotechnical Conference (MELECON)

DOI (link to publication from Publisher):
10.1109/MELECON56669.2024.10608746

Publication date:
2024

Document Version:
Accepted version

Citation for published version (IEEE):
P. Horrillo-Quintero, P. García-Triviño, E. Hosseini, C. A. García-Vázquez, H. Sánchez-Sainz and L. M. Fernández-Ramírez, "Control Scheme for Multi-Energy Microgrids with Power, Heating, Cooling, and Hydrogen Vectors," 2024 IEEE 22nd Mediterranean Electrotechnical Conference (MELECON), Porto, Portugal, 2024, pp. 797-802, doi: 10.1109/MELECON56669.2024.10608746.

Control Scheme for Multi-Energy Microgrids with Power, Heating, Cooling, and Hydrogen Vectors

Pablo Horrillo-Quintero[1], Pablo García-Triviño[1], Ehsan Hosseini[1], Carlos Andrés García-Vázquez[1], Higinio Sánchez-Sainz[2], and Luis M. Fernández-Ramírez[1]

[1] *SURET Reseach Group, Department of Electrical Engineering, University of Cadiz (UCA)*, ETSI Algeciras, Spain

[2] *SURET Reseach Group, Department of Electrical Engineering, University of Cadiz (UCA)*, ESI Puerto Real, Spain

pablo.horrillo@uca.es, pablo.garcia@uca.es, ehsan.hosseini@uca.es, carlosandres.garcia@uca.es, higinio.sanchez@uca.es, luis.fernandez@uca.es

***Abstract*—This paper provides a dynamic control for a multi-energy microgrid (MEMG) comprising heating, cooling, hydrogen, and renewable power vectors connected to a utility grid. A gas boiler is responsible for controlling the hot water thermal bus, whereas an electric boiler manages the hot water demand. An absorption chiller is employed in the cooling circuit to fulfill the cooling load. Furthermore, a battery and a hydrogen system comprising a fuel cell, electrolyzer, and hydrogen tank are considered as energy storage systems (ESSs) for the MEMG. The renewable power is provided through a PV power plant. A new energy management system based on operating states (state-based EMS) is designed to provide three different control scenarios: low temperature (LTM), normal temperature (NTM), and high temperature (HTM). The main target of the presented EMS is to adjust the thermal sources with the aim of avoiding the consumption of the local grid. A 4-hour simulation performed in MATLAB/Simulink, encompassing diverse scenarios, effectively validates the control response of the proposed MEMG. The results illustrated the applicability of this approach within the context of MEMGs.**

Keywords—multi-energy microgrid, dynamic control, power, hydrogen, heating, cooling.

I. INTRODUCTION

A multi-energy microgrid (MEMG) is an energy system that encompasses multiple inputs/outputs combining power, gas, heating, cooling, and hydrogen vectors in a coordinated frame. The deep integration of diverse energy sources and loads in current distribution networks is an inevitable trend in future energy system development [1]. Owing to variations in the progression of unconnected energy systems, energy supply is frequently individually planned, designed, and operated. The absence of coordination among these systems leads to diminished energy utilization rates, reduced overall efficiency, and weakened self-healing capabilities within the energy supply system [2].

Research on MEMG has been carried out from a static perspective, considering a long hourly or diary operating horizon. This traditional approach to MEMG modeling has primarily focused on the optimal power dispatch problem, which aims to minimize a cost function representing the overall energy production costs [3]. However, the applicability of the solutions derived from this analysis could be limited if the operating point of the MEMG components deviates significantly from the linearization point. Unseasonable changes in weather conditions, peak electrical and thermal loads, and dynamic transition states are not considered in this analysis.

This work was partially supported by Ministerio de Ciencia e Innovación, Agencia Estatal de Investigación, and Unión Europea (Grant TED2021-129631B-C32 supported by MCIN/AEI/10.13039/501100011033 and NextGenerationEU/PRTR).

The authors of [4] proposed an optimization algorithm to maximize the utilization of renewable energy sources while minimizing the operating cost based on a linearized coupling model for an MEMG. Nevertheless, it did not consider the dynamic behaviour in the modeling and power dispatching. In [5], three optimization models for power flow were proposed for an IEEE-39 power architecture and 48-node gas distribution network. However, these optimization operations are enclosed within the constraints proposed herein.

In [6], an energy management system (ESS) was employed for a combined power system, heating and cooling. The state of charge (SOC) and capacity optimization of the battery energy storage system (BESS) were selected to optimize the power problem without considering the different time responses between the electrical and thermal components of the system. To address the problem of economic optimization, the authors in [7] presented a green hydrogen storage system to maximize the economic efficiency of a power-to-gas system. Likewise, the proposed benefits are valid within the proposed constraints and do not consider the operating scenarios under extreme conditions. Analogous optimization investigations can be found in [8], [9].

The conversion of electricity to gas was investigated in [10,11] over a daily time horizon, reducing carbon emissions but increasing system operation costs. Demand management for MEMGs was explored in [12] for high-power applications, aiming to optimize the system's load curve. In [13], the optimal placement of ESSs within MEMG was analyzed, although dynamic aspects in their operation were not considered. The optimal integration of MEMGs into energy markets was studied in [14], which facilitated reducing operation costs and meeting local demands.

The studies mentioned above provide evidence of a research gap in the dynamic energy management and control of MEMG. The dynamic perspective provides a new investigation horizon for the coordinated control of several interconnected energy vectors, looking for an efficient energy dispatch in real time. The operating conditions of the MEMG, such as the SOC of the ESS and weather scenarios, and the different time responses of the electrical and thermal dynamics need to be considered to allow a proper control response and extend the operating range beyond linearized models around fixed constraints.

This paper presents a dynamic control scheme for a grid-connected MEMG composed of an electric and gas boilers as thermal sources, and a PV power plant as a renewable source. The ESS consists of a BESS and a hydrogen system formed by a fuel cell, electrolyzer, and hydrogen tank. Additionally, an absorption chiller is considered in the cooling circuit to satisfy the cooling demand. A new state-based EMS is designed to facilitate coordinated operation among various

energy vectors. Three operating modes, denoted as low temperature (LTM), normal temperature (NTM), and high temperature (HTM), are described. The presented EMS dynamically manages the operating states of the thermal sources based on real-time renewable power available to supply the electrical and thermal loads.

The remainder of this article is organised as follows: Section II illustrates the configuration of the MEMG presented. Section III provides the control scheme and energy management system. Section IV collects the results and discussion of the simulations performed. Finally, the conclusions drawn from this paper are set out in Section V.

II. Multi-Energy Microgrid Configuration

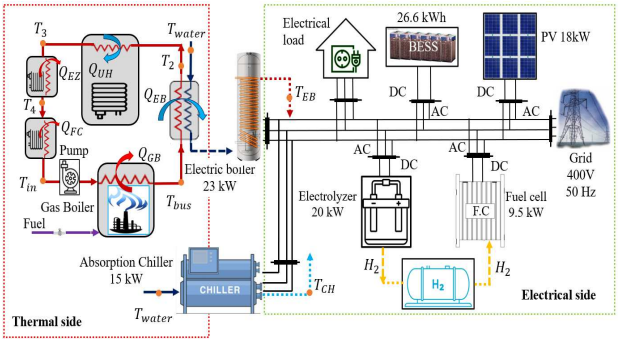

Fig. 1 Schematic configuration of the proposed MEMG.

Fig. 1 represents the MEMG configuration. The thermal side is divided in a hot water circuit and a cooling water circuit. A gas boiler maintains the temperature of the hot thermal bus, while an electric boiler with a rated capacity of 23 kW supplements the system to meet peak hot water demand. Furthermore, the underground heating demand is connected to the hot thermal bus, which represents the household heating demand. The cooling water circuit comprises an absorption chiller with a rated capacity of 15 kW.

The electrical side of the MEMG encompasses a PV power plant with a peak capacity of 18 kWp, an electrical load and a three-phase grid of 400 V. The ESS consists of a Lithium-Ion BESS with a rated capacity of 26.6 kWh and a hydrogen system. The hydrogen system comprises a 20 kW electrolyzer, a 9.5 kW fuel cell and a 1000 kg hydrogen storage tank. The main variables are collected in Table 1.

A. Thermal Vector Modeling

The thermal sources are modeled using the *CARNOT toolbox* from MATLAB/Simulink, developed by the Institute of Solar Research in Juelich, Germany [15]. The gas boiler consists of a multinode model to capture time-dependent conditions, and the dynamic behaviour is governed according to [16,17]:

$$\left(m \cdot c \cdot \frac{1}{N}\right) \cdot \frac{dT_{bus}}{dt} = \left(U \cdot A \cdot \frac{1}{N}\right) \cdot (T_{amb} - T_{bus}) + (\dot{m}_{bus} \cdot c_f) \cdot (T_{in} - T_{bus}) + Q_{GB} \quad (1)$$

The electric boiler is conceptualized as an electric resistive heater that employs electrical energy to elevate the temperature of the incoming mass flow within the water network designated for domestic hot water consumption [16,17]:

TABLE I. Electrical and Thermodinamic Parameters.

Symbol	Parameter	Unit
C_{EB}	Thermal capacity of the boiler	J/K
c	Heat capacity boiler	J/(kg·K)
c_f	Heat capacity of fluid	J/(kg·K)
c_p	Heat capacity of fluid (constant pressure)	J/(kg·K)
E_{BESS}^{nom}	BESS rated capacity	Wh
I_{PV}, I_L, I_{sat}	PV current, light and diode saturation current	A
k	Boltzmann's constant	J/K
m	Mass of the boiler	Kg
$\dot{m}$	Mass flow rate	Kg/s
N	Number of nodes	-
P_{EB}	Electric boiler power	W
$P_{BESS,char}^{max}$	Maximum BESS power in charging mode	W
$P_{BESS,dis}^{max}$	Maximum BESS power in discharging mode	W
Q_{EB}	Heat power of the boiler	W
q	Electron charge	C
R_s, R_{sh}	Series and shunt resistance	(Ω)
T_{amb}	Ambient temperature	ºC
T_{bus}	Bus temperature	ºC
T_{in}	Temperature of fluid at the input	ºC
T_{PV}	PV cell temperature	ºC
UA	Heat loss coefficient to ambient	W/K
V_{PV}	PV voltage	V

$$C_{EB} \cdot \frac{dT_{EB}}{dt} = U \cdot A \cdot (T_{amb} - T_{EB}) + (\dot{m}_{water} \cdot c_p) \cdot (T_{bus} - T_{EB}) + P_{EB} \quad (2)$$

The absorption refrigeration unit relies on the performance curves detailing the cooling capability and efficiency of the reversible air-to-water heat pump utilizing waste heat recovery, specifically the LI 16TER+ model developed by Dimplex [18].

B. Power Vector Modeling

The adoption of the PV system configuration delineated in reference [19] is predicated upon its demonstrated precision and uncomplicated design, as corroborated by previous studies [20]. It is modeled by Equation (3).

$$I_{PV} = I_L - I_{sat}\left(e^{\frac{q(V_{PV}+I_{PV}R_s)}{N_s K T_{PV}}}\right) - (V_{PV} + I_{PV}R_S)/\,R_{sh} \quad (3)$$

The BESS model, originating from the *SimPowerSystems Toolbox* within Simulink [21], has been developed. Rigorous adjustments were undertaken to faithfully represent the Voltage-Current (V-I) and Voltage-State of Charge (V-SOC) curves, along with the dynamic response of the BESS. These modifications were informed by the information extracted from the datasheets to uphold the precision.

C. Hydrogen Vector Modeling

The electrolyzer model employed in this study is based on the proton exchange membrane (PEM) model published in the *Simscape* library [22]. The PEM electrolyzer engages in the utilization of electrical power for the electrolytic dissociation

of water into hydrogen and oxygen. Furthermore, it considers the heat dissipated during the electrolysis process.

The fuel cell model implemented is adopted from the PEM fuel cell model published in [23] from *Simscape* library. The PEM fuel cell produces electrical power through the consumption of hydrogen and oxygen, forming water vapor. Maintaining the optimal temperature and relative humidity in the fuel-cell stack is essential for efficient operation under various loads. Therefore, the heat generated during electrolysis is recovered and recirculated in the hot water circuit.

III. Control Scheme and EMS

The control scheme is shown in Fig. 2. It is remarkable that the controlled components of the MEMG include the electric and gas boilers, along with the absorption chiller. The PV power plant operates at the maximum power point tracking (MPPT) to maximize its output. The ESSs manage the energy balance to avoid the consumption of the local grid. In the case that not ESSs were available, the local grid assumes the surplus or necessary power to fulfill the demand fluctuations.

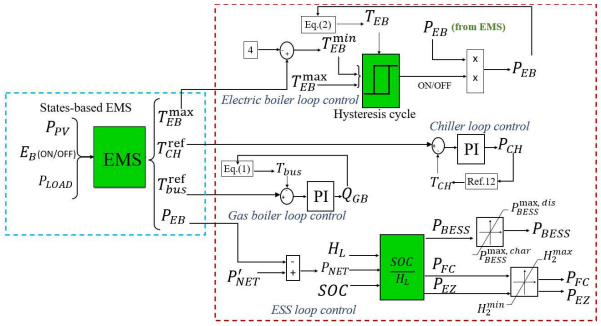

Fig. 2. Overall scheme control.

Four control loops are designed for a proper performance of the MEMG. The electric boiler temperature is controlled through a hysteresis control cycle. The turn off temperature of the hysteresis cycle (T_{EB}^{max}) is provided by the EMS, while the turn on (T_{EB}^{min}) is defined as 4ºC lower than T_{EB}^{max}. The electric boiler is adjusted more efficiently, and no energy is consumed while the hysteresis cycle is decreasing.

The gas boiler control loop controls the hot water circuit thermal bus temperature (T_{bus}). The temperature fluctuates owing to the hot water demand and the underfloor heating demand. Moreover, the heat injected by the gas boiler to achieve the required bus temperature (T_{bus}^{ref}) is regulated employing a PI controller.

In a similar control perspective, a PI-controller is used in the absorption chiller loop control to adjust the chiller consumption (P_{CH}). It receives the water supplied by the local water network and cools in an independent cooling water circuit.

The ESS loop control regulates the energy injected or saved by the BESS and hydrogen system to minimize the reliance on the main grid. In this paper, the energy between the ESSs is distributed according to a rate factor defined as SOC/ H_L . This factor implies that if SOC> H_L , the BESS must deliver more power when operating in the discharging mode. On the other hand, if the ESSs operate in charging mode, the electrolyzer receives more power than the BESS. If SOC< H_L , the power distribution between the ESSs is inversely proportional to that mentioned above.

To extend the useful life of the BESS, a dynamic restriction is established according to the SOC. The maximum power available in discharging ($P_{BESS,dis}^{max}$) or charging $P_{BESS,char}^{max}$ is constrained according to the following equations:

$$P_{BESS,dis}^{max} = min\left(P_{BESS}^{rated}, \frac{E_{BESS}^{nom}}{\Delta t} \cdot \left(\frac{SOC - SOC_{min}}{100}\right)\right) \quad (4)$$

$$P_{BESS,ch}^{max} = min\left(P_{BESS}^{rated}, \frac{E_{BESS}^{nom}}{\Delta t} \cdot \left(\frac{SOC_{max} - SOC}{100}\right)\right) \quad (5)$$

The constraints, Eqs. (4) and (5), define P_{BESS}^{max}, reflecting the BESS maximum power capacity. P_{BESS}^{max} aligns with the BESS rated power and adheres to SOC restrictions, maintaining the SOC within defined upper and lower limits (SOC_{max}, SOC_{min}) . These limits are 90% and 30%, respectively, to ensure safe operation. The discharging adheres to proportional limits between 30% and 50% SOC. Furthermore, the hydrogen tank is limited to 10% and 100% of its capacity, respectively.

A state-base EMS is defined to manage the operating mode of the MEMG. It receives three inputs: the PV power (P_{PV}), the electric load (P_{LOAD}) and the operating mode of the electric boiler, $E_B(ON/OFF)$. The EMS computes four outputs: the turn off temperature of the hysteresis cycle (T_{EB}^{max}), the reference temperature for the absorption chiller (T_{CH}^{ref}), the reference temperature for the hot water circuit bus (T_{bus}^{ref}) and the electric boiler power (P_{EB}).

Fig. 3 depicts the flowchart of the state-based EMS. It is based on the gross net power (P'_{NET}) and the net power (P_{NET}), defined by Eqs. (6) and (7):

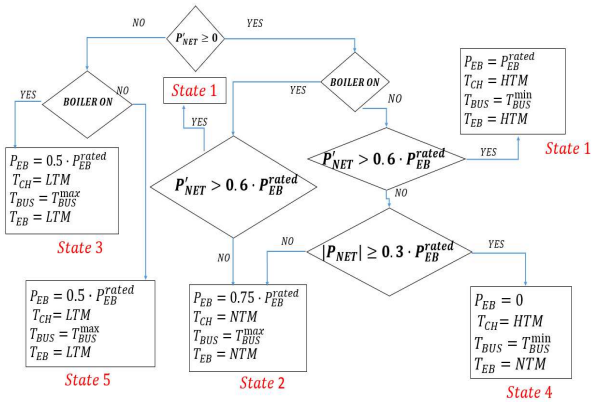

Fig. 3 State-base EMS flowchart.

$$P'_{NET} = P_{PV} - P_{LOAD} \quad (6)$$

$$P_{NET} = P'_{NET} - P_{EB} - P_{CH} \quad (7)$$

where P_{NET} denotes the power that the ESSs must manage with the aim to avoid the consumption of the local grid.

Three operating modes are described, denoted as LTM, NTM and NTM according to the following definitions:

- High-temperature mode (HTM): In instancies where P'_{NET} > 0 and P'_{NET}> 0.6·P_{EB}, the system functions with a surplus of renewable energy. Consequently, the electric boiler turns on the HTM, the gas boiler operates at a reduced

temperature, and the absorption chiller is activated at low temperatures. The surplus renewable energy is overseen by the ESSs and engages in charging mode based on the SOC and the hydrogen level tank (H_L).

- Normal-temperature configuration (NTM): When $P'_{NET} > 0$ and $P'_{NET} < 0.6 \cdot P_{EB}$, the electric boiler is configured in an NTM along with the absorption chiller, the gas boiler elevates its temperature. The ESSs are discharged to satisfy the electrical demand. Additionally, if the electric boiler is deactivated, and $P_{NET} < 0.3 \cdot P_{EB}$, the electric boiler operates according this scenario.
- Low-temperature configuration (LTM): In the event of $P'_{NET} < 0$, the electric boiler is activated under low temperature, whereas the gas boiler and the absorption chiller raise their temperature, as in the NTM. The electric boiler operates at half rated power in this operating mode.

IV. Simulations Results and Discussion

This section evaluates effectiveness of the EMS for the MEMG presented in this paper.

Unlike most articles that focus their efforts on day or week-long horizons, this article proposes the dynamic study of MEMG in a short-hour horizon. To properly observe the behavior of the different equipment under changing operating conditions, a 4-hour study horizon is adopted to adequately represent both the faster thermal dynamics and the slower thermal dynamics.

The 4-hour simulation has been considered in MATLAB/Simulink considering multiple changes in weather conditions, water mass flow, and underfloor heating demand to probe the control system under several scenarios.

The initial SOC for the BESS is selected at 65% and the initial hydrogen level tank (H_L) is set at 50%. Fig. 4 represents the inputs variables to the MEMG, which are the irradiation, the hot water mass flow ($\dot{m}$) and the underfloor heating demand profile (Q_{UH}).

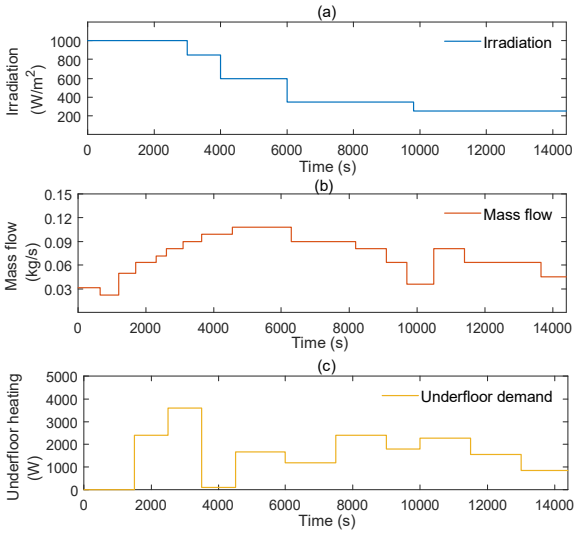

Fig. 4. (a) PV power plant irradiation, (b) thermal power supplied by the electric boiler ($\dot{m}$) and (c) thermal underfloor heating demand (Q_{UH}).

The temperature control of the MEMG is shown in Fig. 5. Fig. 5a depicts the temperature output for the electric boiler

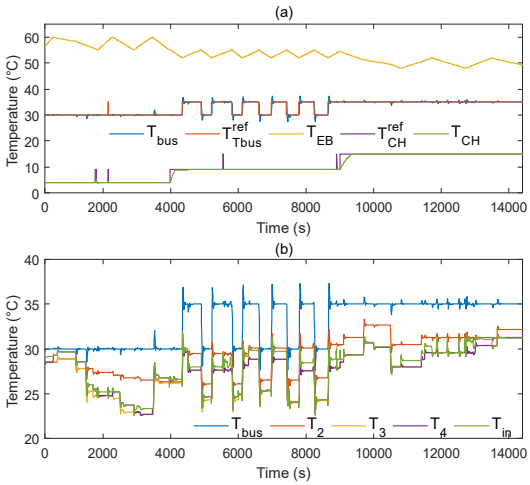

Fig. 5. (a) Thermal bus temperature (T_{bus}), reference temperature of thermal bus (T_{bus}^{ref}), electric boiler temperature (T_{EB}), absorption chiller temperature (T_{CH}), reference temperature of absorption chiller (T_{CH}^{ref}), (b) Nodes temperatures: Bus temperature (T_{bus}), electric boiler output (T_2), underfloor heating output (T_3), electrolyzer output temperature (T_4) and fuel cell output temperature (T_{in}).

(T_{EB}), the bus temperature (T_{bus}), the reference bus temperature value (T_{bus}^{ref}), the absorption chiller output temperature (T_{CH}), and the reference chiller temperature value (T_{CH}^{ref}). From 0 to 4000s, the MEMG operates at the HTM. In this scenario, the hysteresis control cycle for the electric boiler regulates the hot water temperature from 60ºC to 56ºC, T_{bus} is controlled at 30ºC and T_{CH} is set at 4ºC.

When the irradiation drops to 600 W/m^2 at 4000s, the MEMG changes its operation mode to NTM. In this scenario, the electric boiler temperature is controlled from 55ºC to 51ºC, the gas boiler alternates between 35ºC when the electric boiler is turned on and 30ºC when it is turned off, resulting in lower electric consumption. The chiller rises its temperature control to 9ºC. Finally, at 9000s, P_{LOAD} increases its value and the MEMG switches its operating mode to HTM. In this scenario, the electric boiler decreases its temperature from 51ºC to 47ºC, T_{bus} is fixed at 35ºC and T_{CH} at 15ºC. Thus, a proper temperature control is achieved regarding the renewable power and the electric load.

Fig. 5b shows the nodes temperatures of the MEMG. The temperature drops because of the heat extracted from the bus. It is represented the temperature after the hot water exchange (T_2) and the underfloor heating demand (T_3). Due to the heat recovered by the fuel cell and the electrolyzer, the temperature of the bus increases. The increment in the temperature after the fuel cell exchange (T_4) and in the electrolyzer exchange (T_{in}) allows for a lower gas consumption to maintain the bus temperature.

The electrical energy balance is represented in Fig. 6a. It is noteworthy that positive values represent that the energy is supplied, while if the energy is consumed, the values are negative. As seen, from 0 to 4000s, P_{PV} takes a value of 18 kW, P_{LOAD} is set at -1kW and P_{CH} demands -4.5 kW. In these conditions, the MEMG operates at HTM as mentioned above. The electric boiler operates according to its hysteresis cycle at rated power (23 kW). The ESSs distribute the required energy according to the rate between the SOC and H_L. As can be

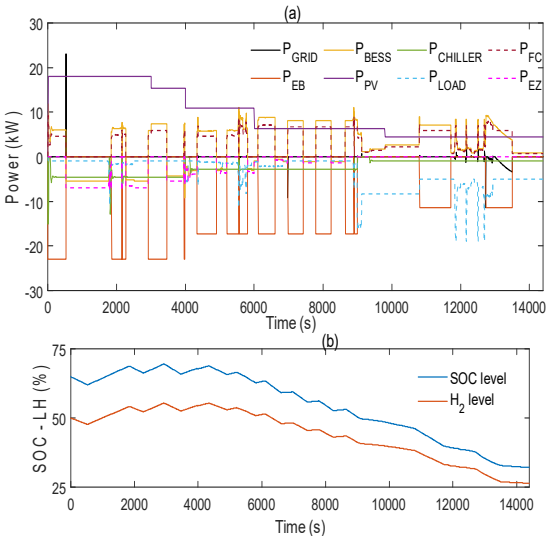

Fig. 6. (a) Electric power balance for the MEMG, and (b) SOC of the BESS and hydrogen level (H_L).

observed, $P_{BESS}^{dis} > P_{FC}$ owing to SOC > H_L. When the electric boiler is off, the surplus energy satisfies $P_{BESS}^{cha} < P_{EZ}$.

The MEMG changes its operation to NTM at 6000s due to the energy reduction in the PV power plant. To minimize the reliance on the main grid, the electric boiler reduces its power to 0.75 of its rated power. The ESSs kept the energy balance and change its operation mode from discharging to charging according to the EMS references. Finally, it is seen at 9000s, that P_{LOAD} takes a peak value of -15 kW. Under this new scenario, the MEMG changes its operating mode to LTM. The electric boiler again reduces its power to 0.5 of its rated power, and the ESSs operate in the discharging mode. It is noted that when the SOC is close to 30%, it cannot supply enough power and the grid deliver the required energy.

Fig 6.b shows the SOC level of the BESS and the H_2 level of the tank. The evolution of these parameters is governed by the electric energy balance, considering proper energy dispatch. It is noteworthy that when the SOC is near 30%, the BESS power is reduced to not exceed this limit and extend the BESS useful life.

Finally, Fig. 7a shows the thermal energy balance of MEMG. In this regard, to maintain T_{bus} at the required reference value, it is needed that the energy injected to the bus (Q_{GEN}) must be equal to the heat extracted from the bus (Q_{CON}). There are three components that inject heat to the bus, which are the gas boiler, the fuel cell and the electrolyzer. On the other side, the heat extracted from the bus is due the hot water demand and the underfloor demand.

The heat recovered in the electrolysis process from the fuel cell (Q_{FC}) and electrolyzer (Q_{EZ}) are shown in Fig. 7b. It represents a mean of a 10% of the electric power for the fuel cell and the electrolyzer, which means that at least 20% of the energy needed to maintain the bus temperature is saved from the gas boiler. Finally, Fig. 7c depicts the heat needed to meet the hot water demand (Q_{EB}) for the three operating modes by the electric boiler.

The results illustrate that the proposed EMS exhibits a satisfactory response, and the MEMG performs adequately, effectively adjusting the operating conditions of the gas and

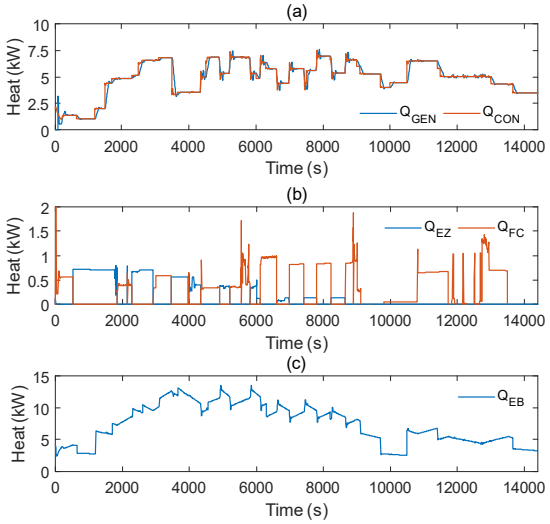

Fig. 7. (a) Thermal power generated (Q_{GEN}) and thermal power consumed (Q_{CON}) , (b) thermal power injected by the electrolyzer (Q_{EZ}) and thermal power injected by the fuel cell (Q_{FC}), and (c) thermal power supplied by the electric boiler (Q_{EB}),

electric boilers to accommodate high, normal, and low-temperature conditions.

V. Conclusions

This paper presented a control scheme for a MEMG with the aim of filling the gap of the dynamic approach of multiple energy vectors in a coordinated operating mode. The MEMG comprises heating, cooling, renewable power and hydrogen vectors.

The control configuration is based on four independent control loops for each thermal source. A new state-base EMS has been presented to manage an electric and gas boilers and an absorption chiller to avoid the consumption from the local grid.

Thermal sources are dynamically regulated based on real-time renewable power availability at each moment. A dynamic constraint was established for the SOC of the BESS to regulate the maximum power that the BESS can manage, and extend the BESS lifespan. It has been probed that the heat generated during the electrolysis can be recovered and injected to the hot thermal water circuit to reduce the gas consumption. A proportional distribution between the SOC and the hydrogen level was considered to perform the energy sharing in the ESSs.

The control scheme has been tested under several scenarios, including diverse weather conditions, peak thermal and electrical demands and variable loads. The results validated the control response achieved and the effectiveness of the MEMG, minimizing the energy injected by the main grid to supply the thermal and electrical loads.

The proposed EMS can benefit distributed system operators by providing efficient energy management of uncontrollable renewable sources and their complementarity with ESSs. Similarly, due to the synergy in the dynamic operation of electricity, hydrogen, and thermal (heating and cooling) vectors, distribution network operators can benefit from having control tools to optimize operation. Moreover, end consumers can also benefit from having energy control and management systems with multiple involved vectors, as it

offers them the possibility to manage energy generation and storage according to their needs, achieving greater independence and exerting their influence buying and selling energy.

REFERENCES

[1] Yu Han, Ke Peng, J. Wang, b. Xu et al., "Research status andprospect of key technologies for coordinated control of multienergy synergic integrated energy systems," Electric Power Construction, vol. 39, no. 12, pp. 81–87, 2018. 10.3969/j.issn.1000-7229.2018.12.010

[2] M. Mou, Y. Zhou, W. Zheng, Z. Zhang, D. Lin, and D. Ke, "Real-Time Optimal Control Strategy for Multienergy Complementary Microgrid System Based on Double-Layer Nondominated Sorting Genetic Algorithm," Complexity, vol. 2020, 2020, doi: 10.1155/2020/8852186.

[3] L. Tan, P. Wang, W. Wang, and D. Xu, "Optimal Operation of Multi-energy Complementary Microgrid with Cooling, Thermal and Electricity Load," in 2021 3rd Asia Energy and Electrical Engineering Symposium, AEEES 2021, Institute of Electrical and Electronics Engineers Inc., Mar. 2021, pp. 599–604. doi: 10.1109/AEEES51875.2021.9403220.

[4] J. Liu, A. Wang, Y. Qu, and W. Wang, "Coordinated Operation of Multi-Integrated Energy System Based on Linear Weighted Sum and Grasshopper Optimization Algorithm," IEEE Access, vol. 6, pp. 42186–42195, Jul. 2018, doi: 10.1109/ACCESS.2018.2859816.

[5] S. Chen, Z. Wei, G. Sun, K. W. Cheung, and D. Wang, "Identifying Optimal Energy Flow Solvability in Electricity-Gas Integrated Energy Systems," IEEE Trans Sustain Energy, vol. 8, no. 2, pp. 846–854, Apr. 2017, doi: 10.1109/TSTE.2016.2623631.

[6] H. Wang et al., "The capacity optimization of the battery energy storage system in the combined cooling, heating and power microgrid," Energy Reports, vol. 9, pp. 567–574, Sep. 2023, doi: 10.1016/j.egyr.2023.04.055.

[7] R. Qiu, H. Zhang, G. Wang, Y. Liang, and J. Yan, "Green hydrogen-based energy storage service via power-to-gas technologies integrated with multi-energy microgrid," Appl Energy, vol. 350, Nov. 2023, doi: 10.1016/j.apenergy.2023.121716.

[8] Z. Zhang, F. M. A. Altalbawy, M. Al-Bahrani, and Y. Riadi, "Regret-based multi-objective optimization of carbon capture facility in CHP-based microgrid with carbon dioxide cycling," J Clean Prod, vol. 384, Jan. 2023, doi: 10.1016/j.jclepro.2022.135632.

[9] R. Chang, Yan Xu, and A. Fars, "Optimal day-ahead energy planning of multi-energy microgrids considering energy storage and demand response," Int J Hydrogen Energy, vol. 48, no. 58, pp. 22231–22249, Jul. 2023, doi: 10.1016/j.ijhydene.2023.03.081.

[10] R. Qiu, H. Zhang, G. Wang, Y. Liang, and J. Yan, "Green hydrogen-based energy storage service via power-to-gas technologies integrated with multi-energy microgrid," Appl Energy, vol. 350, Nov. 2023, doi: 10.1016/j.apenergy.2023.121716.

[11] L. Zhang, Q. Jin, W. Zhang, L. Chen, N. Yang, and B. Chen, "Risk-involved dominant optimization of multi-energy CCHP-P2G-based microgrids integrated with a variety of storage technologies," J Energy Storage, vol. 80, Mar. 2024, doi: 10.1016/j.est.2023.110260.

[12] Y. Nie, Y. Qiu, A. Yang, and Y. Zhao, "Risk-limiting dispatching strategy considering demand response in multi-energy microgrids," Appl Energy, vol. 353, Jan. 2024, doi: 10.1016/j.apenergy.2023.122088.

[13] V. Shahbazbegian, F. Dehghani, M. A. Shafiyi, M. Shafie-khah, H. Laaksonen, and H. Ameli, "Techno-economic assessment of energy storage systems in multi-energy microgrids utilizing decomposition methodology," Energy, vol. 283, Nov. 2023, doi: 10.1016/j.energy.2023.128430.

[14] Q. Y. Wang, X. L. Lv, and A. Zeman, "Optimization of a multi-energy microgrid in the presence of energy storage and conversion devices by using an improved gray wolf algorithm," Appl Therm Eng, vol. 234, Nov. 2023, doi: 10.1016/j.applthermaleng.2023.121141.

[15] Solar Institut Jülich, CARNOT – Conventional And Renewable eNergy CARNOT – Conventional And Renewable Energy Systems OptimizationToolbox.

[16] S. Lohmann, "Einführung in die Software MATLAB® - Simulink® und die Toolboxen CARNOT und Stateflow® zur Simulation von Gebäude- und Heizungstechnik,"

[17] G. Salvadori, L. Ferrari, L. Romano and F. Fantozzi, "Use of CARNOT Toolbox to Evaluate the Impact of Building Automation and Control Systems on Energy and CO2 Emission Savings," 2020 IEEE International Conference on Environment and Electrical Engineering and 2020 IEEE Industrial and Commercial Power Systems Europe (EEEIC / I&CPS Europe), Madrid, Spain, 2020, pp. 1-6, doi: 10.1109/EEEIC/ICPSEurope49358.2020.9160742.

[18] P. Heizen and K. mit Dimplex Wärmepumpen, "PHB_WP_Heizen_Kuehlen_ES." [Online]. Available: www.dimplex.de

[19] W. De Soto, S. A. Klein, and W. A. Beckman, "Improvement and validation of a model for photovoltaic array performance," Sol Energy 2006;80(1):78–88. https://doi.org/ 10.1016/j.solener.2005.06.010.

[20] M. G. Villalva, J. R. Gazoli, and E. R. Filho, "Comprehensive approach to modeling and simulation of photovoltaic arrays," IEEE Trans Power Electron 2009;24(5): 1198–208. https://doi.org/10.1109/TPEL.2009.2013862.

[21] SimPowerSystems TM. Reference. Natick, MA: Hydro-Quebec and the MathWorks. Inc; 2015.

[22] The MathWorks, Inc. "PEM Electrolysis System" mathworks.com. Accessed: January 03, 2024. [Online]. Available: https://www.mathworks.com/help/stats/index.html.

[23] The MathWorks, Inc. "PEM Fuell System" mathworks.com. Accessed: January 03, 2024. [Online]. Available: https://es.mathworks.com/help/simscape/ug/pem-fuel-cell-system.html?lang=en.